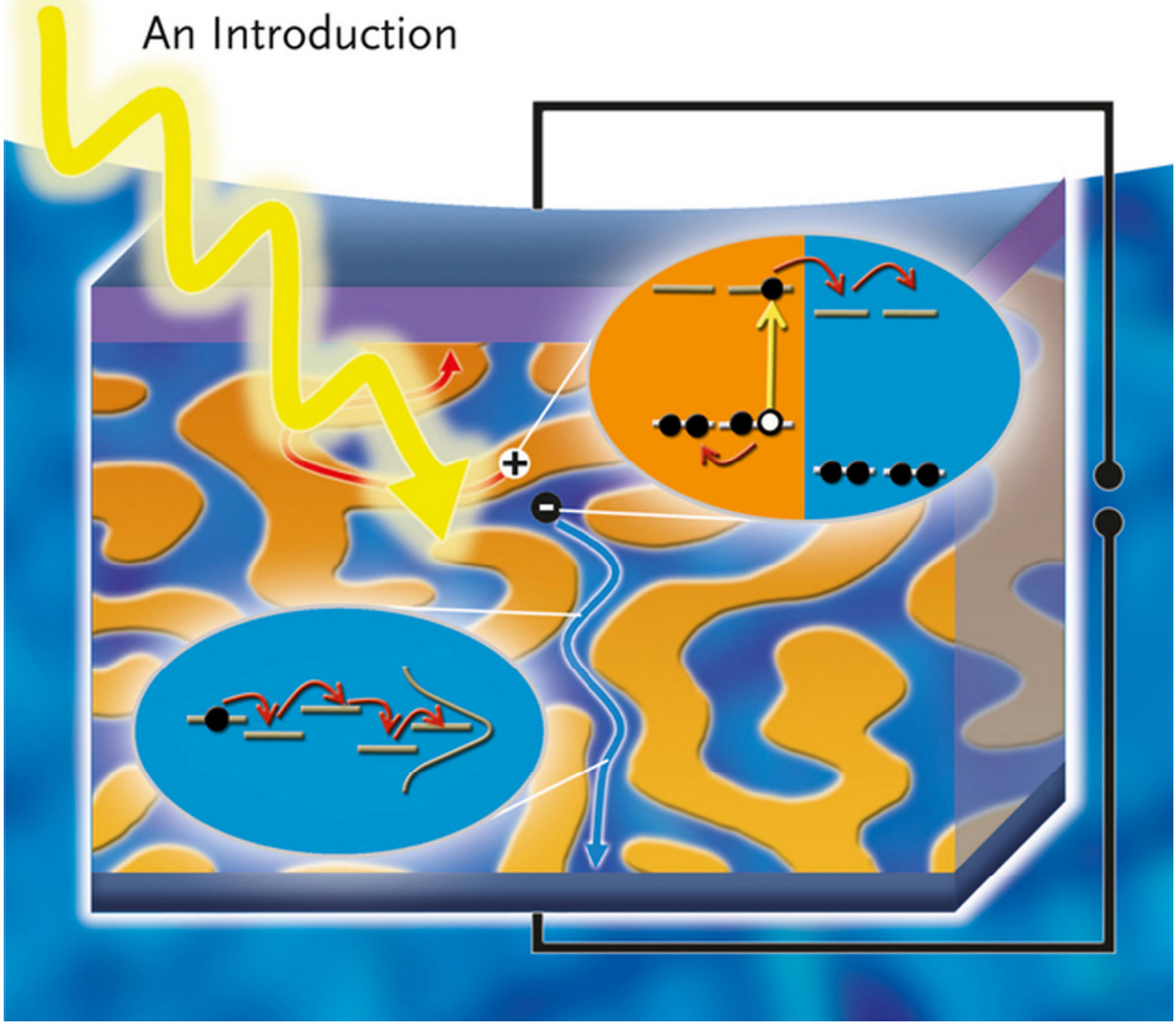
WILEY-VCH

Anna Köhler and Heinz Bässler

Electronic Processes in Organic Semiconductors

An Introduction



Anna Köhler and
Heinz Bässler

Electronic Processes in Organic Semiconductors

Related Titles

Brütting, W., Adachi, C. (eds.)

Physics of Organic Semiconductors

Second Edition
2012
Print ISBN: 978-3-527-41053-8 (Also available in a variety of electronic formats)

Valeur, B., Berberan-Santos, M.N.

Molecular Fluorescence
Principles and Applications

Second Edition
2012
Print ISBN: 978-3-527-32837-6 (Also available in a variety of electronic formats)

Tsujimura, T.

OLED displays fundamentals and applications

2012
Print ISBN: 978-1-118-17306-0

Klauk, H. (ed.)

Organic Electronics II
More Materials and Applications

2012
Print ISBN: 978-3-527-32647-1 (Also available in a variety of electronic formats)

Li, Q. (ed.)

Self-Organized Organic Semiconductors
From Materials to Device Applications

2011
Print ISBN: 978-0-470-55973-4 (Also available in a variety of electronic formats)

Hadziioannou, G., Malliaras, G. G. (eds.)

Semiconducting Polymers
Chemistry, Physics and Engineering

Second, Completely Revised and Enlarged Edition
2007
Print ISBN: 978-3-527-31271-9

Lanzani, G.

The Photophysics behind Photovoltaics and Photonics

2012
Print ISBN: 978-3-527-41054-5

Schwoerer, M., Wolf, H. C.

Organische Molekulare Festkörper
Einführung in die Physik von pi-Systemen

2005
Print ISBN: 978-3-527-40539-8

Anna Köhler and
Heinz Bässler

Electronic Processes in Organic Semiconductors

An Introduction

WILEY-VCH
Verlag GmbH & Co. KGaA

Samsung Exhibit 1058, Page 4 of 33
Samsung v. W&Wsens - PGR2025-00082

The Authors

Prof. Dr. Anna Köhler
Universität Bayreuth
Experimentalphysik II
Universitätsstr. 30
95447 Bayreuth
Germany

Prof. Dr. Heinz Bässler
Universität Bayreuth
Bayreuther Institut für
Makromolekülforschung (BIMF)
Universitätsstr. 30
95447 Bayreuth
Germany

Cover
The cover shows a cross-section through a bulk heterojunction solar cell. The simplified schematics illustrate the photogeneration and transport of charges.

All books published by **Wiley-VCH** are carefully produced. Nevertheless, authors, editors, and publisher do not warrant the information contained in these books, including this book, to be free of errors. Readers are advised to keep in mind that statements, data, illustrations, procedural details or other items may inadvertently be inaccurate.

Library of Congress Card No.: applied for

British Library Cataloguing-in-Publication Data
A catalogue record for this book is available from the British Library.

Bibliographic information published by the Deutsche Nationalbibliothek
The Deutsche Nationalbibliothek lists this publication in the Deutsche Nationalbibliografie; detailed bibliographic data are available on the Internet at <http://dnb.d-nb.de>.

© 2015 Wiley-VCH Verlag GmbH & Co. KGaA, Boschstr. 12, 69469 Weinheim, Germany

All rights reserved (including those of translation into other languages). No part of this book may be reproduced in any form – by photoprinting, microfilm, or any other means – nor transmitted or translated into a machine language without written permission from the publishers. Registered names, trademarks, etc. used in this book, even when not specifically marked as such, are not to be considered unprotected by law.

Print ISBN: 978-3-527-33292-2
ePDF ISBN: 978-3-527-68514-1
ePub ISBN: 978-3-527-68516-5
Mobi ISBN: 978-3-527-68515-8
oBook ISBN: 978-3-527-68517-2

Cover Design Adam Design, Weinheim, Germany
Typesetting Laserwords Private Limited, Chennai, India
Printing and Binding Markono Print Media Pte Ltd., Singapore

Printed on acid-free paper

Contents

Preface *XI*
Table of Boxes *XIII*

1 The Electronic Structure of Organic Semiconductors *1*
1.1 Introduction *1*
1.1.1 What Are "Organic Semiconductors"? *1*
1.1.2 Historical Context *3*
1.2 Different Organic Semiconductor Materials *5*
1.2.1 Molecular Crystals *5*
1.2.2 Amorphous Molecular Films *7*
1.2.3 Polymer Films *9*
1.2.4 Further Related Compounds *14*
1.2.5 A Comment on Synthetic Approaches *15*
1.3 Electronic States of a Molecule *17*
1.3.1 Atomic Orbitals in Carbon *17*
1.3.2 From Atomic Orbitals to Molecular Orbitals *19*
1.3.3 From Orbitals to States *25*
1.3.4 Singlet and Triplet States *28*
1.4 Transitions between Molecular States *31*
1.4.1 The Potential Energy Curve *31*
1.4.2 Radiative Transitions: Absorption and Emission *37*
1.4.2.1 The Electronic Factor *38*
1.4.2.2 The Vibrational Factor *41*
1.4.2.3 The Spin Factor *45*
1.4.3 A Classical Picture of Light Absorption *48*
1.4.3.1 The Lorentz Oscillator Model and the Complex Refractive Index *48*
1.4.3.2 Relating Experimental and Quantum Mechanical Quantities: The Einstein Coefficients, the Strickler–Berg Expression, and the Oscillator Strength *52*
1.4.4 Non-Radiative Transitions: Internal Conversion and Intersystem Crossing *56*
1.4.4.1 The Franck–Condon Factor *F* and the Energy Gap Law *57*
1.4.4.2 The Electronic Coupling J *58*
1.4.4.3 Accepting Modes, Promoting Modes, and the Isotope Rule *59*
1.4.4.4 Implications of the Energy Gap Law *60*
1.4.4.5 The Strong Coupling Limit *61*
1.4.5 Basic Photophysical Parameters: Lifetimes and Quantum Yields *62*
1.5 Spectroscopic Methods *64*
1.5.1 Photoluminescence Spectra, Lifetimes, and Quantum Yields *67*
1.5.1.1 Steady State Spectra and Quantum Yields *68*

Samsung Exhibit 1058, Page 6 of 33
Samsung v. W&Wsens - PGR2025-00082

1.5.1.2 Spectra and Lifetimes in the Nanosecond to Second Range *72*
1.5.1.3 Spectra and Lifetimes in the Picosecond to Nanosecond Range *73*
1.5.1.4 Spectra and Time Scales below the Picosecond Range *74*
1.5.2 Excited State Absorption Spectra *75*
1.5.2.1 Steady State Spectra (Photoinduced Absorption) *75*
1.5.2.2 Spectra in the Nanosecond Range (Flash Photolysis) *77*
1.5.2.3 Spectra in the Femtosecond Range (fs Pump–Probe Measurements) *78*
1.5.3 Fluorescence Excitation Spectroscopy *79*
1.6 Further Reading *80*
References *81*

2 Charges and Excited States in Organic Semiconductors *87*
2.1 Excited Molecules from the Gas Phase to the Amorphous Film *87*
2.1.1 Effects due to Polarization *87*
2.1.2 Effects due to Statistical Averaging *91*
2.1.3 Effects due to Environmental Dynamics *94*
2.1.4 Effects due to Electronic Coupling between Identical Molecules – Dimers and Excimers *99*
2.1.4.1 Electronic Interaction in the Ground State *99*
2.1.4.2 Electronic Interaction in the Excited State *99*
2.1.4.3 Oscillator Strength of Dimer and Excimer Transitions *105*
2.1.4.4 Singlet and Triplet Dimers/Excimers *107*
2.1.5 Effects due to Electronic Coupling between Dissimilar Molecules – Complexes and Exciplexes *111*
2.1.6 Electromers and Electroplexes *113*
2.2 Excited Molecules in Crystalline Phases – The Frenkel Exciton *114*
2.2.1 The Frenkel Exciton Concept for One Molecule per Unit Cell *114*
2.2.2 The Frenkel Exciton Concept for Two Molecules per Unit Cell *117*
2.2.3 Coherent and Incoherent Motion of Frenkel Excitons *118*
2.2.4 Förster and Dexter Type Energy Transfer *119*
2.2.5 Experimental Examples for Frenkel Excitons in Ordered Molecular Arrays *123*
2.2.5.1 Molecular Crystals: Anthracene and Tetracene *123*
2.2.5.2 Cyclic Arrays of Chromophores: Light-Harvesting Proteins *124*
2.2.5.3 Molecular J and H Aggregates: Cyanine Dyes and Carotenes *126*
2.2.5.4 Weakly Interacting H and J Aggregates with Vibronic Coupling *127*
2.3 Excited States in π-Conjugated Polymers *133*
2.3.1 Crystalline Polymers: Poly(diacetylene)s (PDAs) *133*
2.3.2 Concepts for Noncrystalline Polymers *136*
2.3.2.1 The Basic Idea *136*
2.3.2.2 Quantitative Approaches: Exciton Models *141*
2.3.2.3 Comparison Against Experimental Data *143*
2.3.3 Brief Overview Over Different Classes of Conjugated Polymers *144*
2.3.3.1 Poly(ene)s/Poly(acetylene)s *144*
2.3.3.2 Poly(*p*-phenylene vinylenes) *147*
2.3.3.3 Poly(*p*-phenylene)s *150*
2.3.3.4 Poly(thiophene)s *152*
2.3.3.5 Poly(silane)s/Poly(silylene)s *153*
2.3.3.6 Low-Gap Donor–Acceptor Polymers *154*
2.4 Charged Molecules *155*
2.4.1 The Creation of Charged Molecules by Injection, Absorption and Doping *157*
2.4.1.1 By Injection *157*

2.4.1.2 By Absorption *158*
2.4.1.3 By Doping *159*
2.4.2 Charged Molecules in Disordered Films *161*
2.4.2.1 The Energy of Charged Molecules *161*
2.4.2.2 The Absorption of Charged Molecules *162*
2.4.3 Charged Molecules in Crystals *164*
2.4.4 Determining the Energy Levels of Charged Molecules by Cyclovoltammetry and Photoemission Spectroscopy *167*
2.4.4.1 Cyclovoltammetry *167*
2.4.4.2 Photoemission Spectroscopy (UPS, XPS, IPES) *169*
2.4.4.3 The Difference between Electrical Gap and Optical Gap *170*
2.5 A Comparison between Inorganic and Organic Semiconductors *171*
2.5.1 Crystals *171*
2.5.2 Amorphous Solids *174*
2.5.3 The Su–Schrieffer–Heeger (SSH) Model for Conjugated Polymers *175*
2.6 Further Reading *181*
References *182*

3 Electronic and Optical Processes of Organic Semiconductors *193*
3.1 Basic Aspects of Electrical Current in a Device *194*
3.1.1 Injection Limited Currents *195*
3.1.2 Unipolar Space Charge Limited (SCL) Current *196*
3.1.3 Bipolar Space Charge Limited Current *200*
3.2 Charge Injection Mechanisms *201*
3.2.1 Fowler–Nordheim Tunneling Injection *202*
3.2.2 Richardson–Schottky Thermionic Injection *203*
3.2.3 Thermally Activated Injection into a Disordered Organic Semiconductor *204*
3.3 Charge Carrier Transport *208*
3.3.1 Experimental Techniques to Measure Charge Carrier Mobility *208*
3.3.1.1 The Time of Flight Technique *208*
3.3.1.2 Space-Charge-Limited Currents (SCLC) *209*
3.3.1.3 Carrier Extraction by Linearly Increasing Voltage (CELIV) *210*
3.3.1.4 Field-Effect Transistors (FETs) *211*
3.3.1.5 Time-Resolved Microwave Conductivity (TRMC) *212*
3.3.1.6 Terahertz Spectroscopy *212*
3.3.1.7 Optical Probing *213*
3.3.2 Carrier Transport in the Band Regime and in the Hopping Regime *213*
3.3.2.1 Band Transport *215*
3.3.2.2 Hopping Transport *217*
3.3.2.3 Polaronic Transport *217*
3.3.2.4 Disorder-Controlled Transport *223*
3.3.2.5 Superposition of Polaron and Disorder Effects *233*
3.3.3 Trapping Effects *235*
3.3.4 Transport at Higher Charge Carrier Densities *237*
3.3.5 The Impact of Morphology on Transport *239*
3.3.5.1 The Influence of Excimers and Traps *239*
3.3.5.2 The Role of Aggregates and Crystallites *240*
3.3.5.3 Self-Ordering in Discotic Liquid Crystals *241*
3.3.5.4 Polycrystalline Films *243*
3.3.6 Charge Transport on Short Lengths Scales and Time Scales *244*
3.4 Non-Geminate Charge Carrier Recombination *246*

3.4.1 Recombination without Traps (Langevin-Type Recombination) *246*
3.4.2 Recombination with Traps (Shockley–Read–Hall-Like Recombination) *247*
3.5 Generation of Excitations *249*
3.5.1 Optical Generation *249*
3.5.2 Electrical Generation *251*
3.5.3 Secondary Processes *252*
3.6 Dissociation of Excitations *254*
3.6.1 Geminate Pair Creation *254*
3.6.1.1 The Timescale of Charge Transfer *254*
3.6.1.2 Properties of Geminate Pairs in Single-Compound Materials *256*
3.6.1.3 Geminate Pairs in Materials at an Interface or Containing Traps *259*
3.6.1.4 Geminate Pairs in Donor–Acceptor Systems *260*
3.6.2 The Dissociation of the Geminate Pair *263*
3.6.2.1 The Onsager (1938) Model *263*
3.6.2.2 The Onsager–Braun Model *265*
3.6.2.3 Hong and Noolandi's Time-Dependent Formalism *266*
3.6.2.4 Pump–Push–Probe Experiments to Monitor the Geminate Pair Population *267*
3.6.2.5 Contemporary Models Considering the Effects of Conjugation Lengths *269*
3.6.2.6 The Influence of Disorder on Geminate Pair Dissociation *272*
3.7 Diffusion of Excitations *274*
3.7.1 Exciton Diffusion in a Molecular Crystal *274*
3.7.2 Diffusion of Excitations in Amorphous Condensed Phases *276*
3.7.3 Experimental Techniques to Measure Exciton Diffusion *276*
3.7.3.1 Measuring Diffusion by Luminescence Quenching *276*
3.7.3.2 Monitoring Spectral Diffusion *279*
3.8 Decay of Excitations *283*
3.8.1 Monomolecular Decay *283*
3.8.1.1 Fluorescence *283*
3.8.1.2 Phosphorescence *286*
3.8.2 Bimolecular Processes *287*
3.8.2.1 Singlet-Singlet-Annihilation *288*
3.8.2.2 Triplet–Triplet-Annihilation *288*
3.8.2.3 Triplet-Charge-Annihilation *290*
3.8.2.4 Singlet–Triplet-Annihilation *291*
3.9 Further Reading *292*
References *292*

4 Fundamentals of Organic Semiconductor Devices *307*
4.1 Basic Solar Cells and Light-Emitting Diode Structures *311*
4.1.1 Basic Fabrication Steps *311*
4.1.2 Electrode Geometries *315*
4.1.3 The Basic Operation of a Single-Layer OLED *317*
4.1.4 Multi-Layer OLED Architectures *322*
4.1.5 The Current–Voltage–Luminance Characteristics of an OLED *324*
4.1.6 The Basic Operation of an OSC *326*
4.1.7 The Current–Voltage Characteristics of an OSC *327*
4.2 Solar Cell Performance *331*
4.2.1 Determining Solar Cell Efficiencies *331*
4.2.2 Strategies to Increase the Photocurrent *334*
4.2.2.1 The Bilayer Device *337*
4.2.2.2 The Bulk Heterojunction Device *339*

4.2.2.3 The Multilayer Device *345*
4.2.3 Strategies to Increasing the Open-Circuit Voltage *345*
4.2.4 Strategies to Improve the Fill-Factor *347*
4.2.5 The Thermodynamic Efficiency Limit *349*
4.3 Light-Emitting Diode Performance *353*
4.3.1 Determining OLED Efficiencies and Color *353*
4.3.1.1 Photometric and Radiometric Units *353*
4.3.1.2 Defining Efficiencies *355*
4.3.1.3 Color Coordinates *356*
4.3.1.4 The Color Rendering Index *360*
4.3.1.5 Lifetime Measurements *361*
4.3.2 Strategies to Improve the OLED Efficiencies *362*
4.3.3 Strategies to Improving the Emission Color of OLEDs *366*
4.3.3.1 Single Color OLEDs *366*
4.3.3.2 White Organic Light Emitting Diodes (WOLEDs) *366*
4.4 Transistors *368*
4.4.1 The Operational Principle of an OFET *369*
4.4.2 Evaluating OFET Performance *373*
4.4.3 Improving OFET Performance *374*
4.4.3.1 Choosing Source and Drain Electrodes *374*
4.4.3.2 Choosing the Gate Insulator *375*
4.4.3.3 Improving Charge Transport *377*
4.4.4 Modifying the Polarity of OFETs *378*
4.4.4.1 *n*-Type Transistors *379*
4.4.4.2 Ambipolar Transistors *380*
4.5 Further Reading *382*
References *382*

Appendices *389*
Chemical Structures *389*
A.1 Selected Polymers *390*
A.1.1 π-Conjugated Homopolymers *390*
A.1.2 π-Conjugated Copolymers *391*
A.1.3 Other Polymers of Interest *392*
A.2 Selected π-Conjugated Low-Molecular Weight Compounds *393*
A.3 Selected Phosphorescent Compounds *397*
A.4 Non-Conjugated Low-Molecular Weight Compounds *397*

Index *399*

Preface

Over the past 40 years, the field of organic semiconductors has developed from an a thriving yet small community into a rather large research area. Both, the understanding of the underlying photophysics and device physics as well as the evolution of device technology have come to a mature stage. Despite this progress in science and technology, PhD students in this research field often experience a gap between the knowledge they acquired in the course of their undergraduate studies in physics, engineering, chemistry, or material science, and the knowledge that is needed to tackle a PhD in this subject area. Similarly, scientists entering the field of organic semiconductors with different backgrounds require reading material that familiarizes them with some of the underlying concepts before embarking on their own in-depth study.

Our book aims to bridge this gap by giving a careful introduction into the field, with a focus on the fundamentals. It is based on a lecture course that AK has given for a number of years at the University of Bayreuth to final year undergraduates and Master/PhD Students with a background in physics or chemistry. After having studied our book, the reader should be well-equipped to explore expert reviews and specialized book chapters that discuss a particular aspect of a material, a mechanism, or a device design in greater depth. While it is primarily intended for Master and PhD students requiring a basis for understanding organic semiconductors, we also delineate current routes in research with a view to stimulate scientific curiosity.

The book is structured in four chapters. In Chapter 1, we introduce the reader to basic concepts of molecular photophysics. Thus, we discuss the different types of organic semiconductors, their electronic states, radiative and nonradiative transitions between their states, and how to detect them by spectroscopic means. The way how interactions between chromophores affect charges and excited states is studied in Chapter 2. In particular, we highlight the differences between molecules in the gas phase and in the condensed phase, as well as the effect of structural order on the electronic properties. Dimers, excimers, excitons, and the particular electronic structure of π-conjugated polymers are introduced. For the benefit of those with a background in inorganic semiconductors, we also briefly compare the physics of organic versus inorganic semiconductors. Chapter 3 delineates the processes that are relevant to optoelectronic devices. In particular, the sections on charge carrier transport and on exciton dissociation include recent developments. How these processes can be employed to the fabrication of organic semiconductor devices is presented in Chapter 4.

The text is complemented by boxes. They explore a particular aspect in greater depth or briefly introduce a feature that may be familiar to one group of readers yet not to another group. Where figures show original spectra, they are redrawn to be presented uniformly on an energy scale in electron-volt throughout this book for ease of comparison. A list of chemical structures is given in the appendix for reference. While this textbook is meant to be self-contained, we have included many references to original work as well as a list of further reading at the end of each chapter. Our objective in including original references is to sensitize PhD students to the notion (i) that conceived knowledge is based on experiments and their interpretation, both of which are done by humans, (ii) that there may be some discussion as to the most appropriate interpretation until a canonical view is formed in the course of time, and (iii) that it is a good idea for them to use their own judgment about the original

Samsung Exhibit 1058, Page 11 of 33
Samsung v. W&Wsens - PGR2025-00082

literature to form an opinion, in particular in a field where there still is ongoing development. Our intention was to write an experimentally based, reasonably slim textbook for those new to the field rather than a comprehensive review on the state of the art. Thus, not every piece of work that may be of importance to the field could be included here, and we ask our colleagues to bear with this.

Finally, we take the freedom to highlight here two aspects of science that feel important to us. One is perhaps well expressed in a little anecdote about the German philosopher Georg Wilhelm Friedrich Hegel, who lived from 1770 to 1831. Reportedly, he submitted a thesis for habilitation, "De orbitis planetarum" claiming that on logical grounds there cannot be more than seven planets. His defense was due on 27 August 1801, yet on 1 January 1801, an eighth planet, the Ceres, had been observed. When the issue was raised to Hegel that his model was in contradiction to the facts, he is said to have replied "too bad for the facts." We hope our readers will keep a healthy critical attitude to perceived scientific ideas and an openness to question their own views in the light of new results that may come up.

The second aspect relates to our opinion that an interdisciplinary field such as organic semiconductor requires researchers to take a wide variety of approaches, experimental, theoretical computational, technological, and so on, and that there is no order of priority between them. Obtaining good understanding requires all of these approaches. This is, by the way, not a new phenomenon. When William Shockley gave his Nobel lecture in 11 December 1956 on "Transistor technology evokes new physics," he remarked. "I would like to express some viewpoints about words often used to classify types of research in physics; for example, pure, applied, unrestricted, fundamental, basic, academic, industrial, and practical. It seems to me that all too frequently some of these words are used in a derogatory sense, on the one hand to belittle the practical objectives of producing something useful and, on the other hand, to brush off the possible long-range value of explorations into new areas where a useful outcome cannot be foreseen. Frequently, I have been asked if an experiment I have planned is pure or applied research; to me it is more important to know if the experiment will yield new and probably enduring knowledge about nature. If it is likely to yield such knowledge, it is, in my opinion, good fundamental research." We want to encourage in particular young researchers to be open to any kind of scientific approach that seems promising for their investigations.

This book would not exist without the support of many people. We are indebted to our colleagues in Bayreuth, in particular Stephan Kümmel, Jürgen Köhler, and Mukundan Thelakkat, who generously took over administrative and grant-writing tasks thus giving AK the space and time to actually write the book, and to Peter Strohriegl and Markus Schwoerer for proof-reading and suggestions. We also thank Paul Blom, Frank Spano, Stavros Athanasopoulos, and Dieter Neher for proof-reading and suggestions. All members of AK's research group contributed in one way or another to this book. All of the figures and the draft for the book cover were prepared by Katja Huber, who, together with Julian Kahle also edited the references. Chapters were proof-read mainly by Julian Kahle, Christian Schwarz, Sebastian Hoffmann, Tobias Hahn, and Markus Reichenberger. Steffen Tscheuschner, Fabian Panzer, Christina Scharsich, Alexander Rudnick, and Philipp Knauer provided occasional data, calculations, chemical structures, and technical assistance. We are extremely grateful to the entire group for their help in preparing this book. HB thanks the Bayreuth Institute of Macromolecular Science at the University of Bayreuth for providing office space and infrastructural support and he acknowledges his former research group in Marburg for more than 30 years of research that yielded many fruitful ideas and insight.

Bayreuth, March 2015 *Anna Köhler and Heinz Bässler*

Samsung Exhibit 1058, Page 12 of 33
Samsung v. W&Wsens - PGR2025-00082

Table of Boxes

Box 1.1 Average Molecular Weights of Polymers
Box 1.2 Polymer Structures and Their Names
Box 1.3 σ- and π-Orbitals
Box 1.4 The Energy Levels of the Hydrogen Ion
Box 1.5 Calculating Molecular Orbitals
Box 1.6 Nomenclatures
Box 1.7 The Zero-Field Splitting
Box 1.8 Wavelengths, Wavenumbers, and Energy Conversion Units
Box 1.9 Raman and FTIR Spectroscopy
Box 1.10 Absorption and Oscillator Strength
Box 1.11 Franck–Condon Factors for Displaced and Distorted Oscillators
Box 1.12 Franck–Condon Factors Involving Several Modes
Box 1.13 Solvents and the Hildebrand Solubility Parameter
Box 1.14 Quenching by Molecular Oxygen

Box 2.1 Phonons, Vibrons, and the Electronic Coupling to Them
Box 2.2 Stokes' Shift
Box 2.3 Effective Vibrational Modes
Box 2.4 Electroabsorption
Box 2.5 The Particle-in-a-Box Model Applied to π-Conjugated Oligomers

Box 3.1 Isotropic Diffusion
Box 3.2 Conductivity of a Semiconductor
Box 3.3 Arrhenius Plot
Box 3.4 Interfacial Dipoles Probed by Photoemission Spectroscopy
Box 3.5 Marcus Theory for Electron Transfer
Box 3.6 The Continuous Time RandomWalk (CTRWModel)
Box 3.7 Spectral Diffusion

Box 4.1 The pn Junction and the Shockley Equation
Box 4.2 The Schottky Junction and Band Bending
Box 4.3 Flory Huggins-Theory
Box 4.4 An Eutectic System
Box 4.5 The Shockley–Queisser (Detailed Balance) Limit
Box 4.6 A Microcavity
Box 4.7 Surface Treatments

Samsung Exhibit 1058, Page 13 of 33
Samsung v. W&Wsens - PGR2025-00082

3
Electronic and Optical Processes of Organic Semiconductors

Semiconductors are, by definition, materials that are intended for use in optoelectronic devices. The most common applications of organic semiconductors encompass organic light-emitting diodes (OLEDs), organic solar cells (OSCs), and organic field-effect transistors (OFETs) (Figure 3.1).

In essence, an OLED is made in a sandwich-type structure by covering a substrate sequentially with a bottom electrode, the active semiconducting material and a top electrode. Upon applying a voltage, positive and negative charges are injected from the electrodes into the semiconductor and move through it. While a part of these charges may leave the organic film at the counter electrode, having resulted in nothing but dissipated heat, some of the electrons and holes will encounter and capture each other to form an excited state that may recombine with or without light emission. The processes involved in the operation of an OLED are illustrated in Figure 3.1, along with the processes relevant for an OSC. The OSC has, in principle, the same structure as that of an OLED; yet, it operates in the reverse direction. Light is absorbed and creates excited states. Some of these states may eventually dissociate into free, mobile positive and negative charges that move to opposite electrodes where they are collected to yield a current. The photophysical mechanisms associated with OLEDs and OSC operation, such as charge injection, charge transport, electron–hole recombination, and excited state dissociation are discussed in detail in the corresponding sections of this chapter. Also included are processes relating to the excited states such as energy transfer and decay mechanisms. Issues pertaining to the fabrication, operation, characterization, and optimization of the entire device are considered in the next chapter. The same approach of chapter organization is taken concerning the OFET. The fabrication and operation of the OFET is detailed in Chapter 4, whereas this chapter covers, *inter alia*, the process of charge transport for the regimes of low and high charge carrier density.

The generic structure of an OFET differs from the OLED/OSC structure. An OFET contains three electrodes in contrast to the two electrodes of the OLED/OSC layout. In the OFET, two electrodes, the *source* and the *drain* electrode, are separated by the active semiconductor. When a voltage is applied between the source and the drain electrode, current can, in principle, flow between them. The amount of current that flows is controlled by the third, the *gate* electrode that is separated from the active semiconductor by an insulator layer. If there is no voltage applied to the gate electrode, the current flow between the source and the drain is negligibly small, even when there is a potential difference between the source and the drain. The reason for this lies in the high resistivity of the organic semiconductor in combination with the device geometry. In an OLED, the electrodes are separated only by 100 nm of semiconductor, and the electrodes cover most of the semiconductor surface. A voltage of 1 V, implying a field of 10^{-5} V cm^{-1}, thus suffices to inject enough charges for OLED operation. In contrast in the OFET, source and drain electrodes are separated by about 100 µm and cover only a small fraction of the semiconductor. Even when 10 V are applied, the associated field of 10^{3} V cm^{-1} is insufficient to result in significant charge injection and thus current. A higher charge density can be obtained by applying a voltage to the gate electrode. Charges then accumulate at the semiconductor/dielectric interface, thus rendering the organic semiconductor more conductive. As a result, current flow from source to drain is now significantly enhanced.

Electronic Processes in Organic Semiconductors, First Edition. Anna Köhler and Heinz Bässler.
© 2015 Wiley-VCH Verlag GmbH & Co. KGaA. Published 2015 by Wiley-VCH Verlag GmbH & Co. KGaA.

Samsung Exhibit 1058, Page 14 of 33
Samsung v. W&Wsens - PGR2025-00082

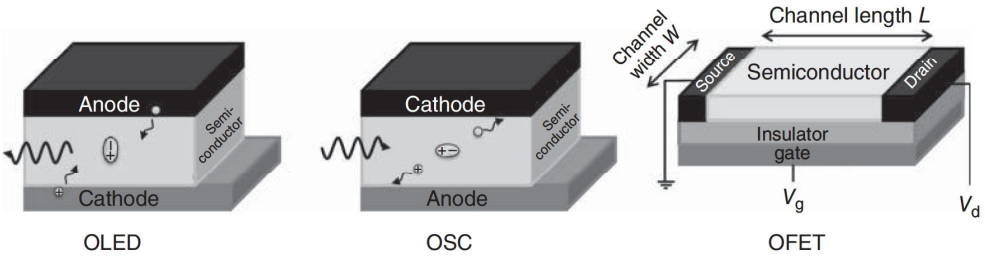


Figure 3.1 Schematic of an OLED, OSC, and OFET. The processes of charge injection, recombination and light emission are illustrated for the OLED. Similarly for the OSC, light absorption, exciton dissociation, and electron collection at the electrodes are shown schematically. In the OFET, current flow from source to drain electrode though the semiconductor channel is controlled by the gate electrode.

This brief exposition on the operation of OLEDs, OSCs, and OFETs may suffice to illustrate the need for a detailed and more profound understanding of the underlying photophysical processes.

3.1 Basic Aspects of Electrical Current in a Device

The electric current flowing through a device in the dark can be limited by either the efficiency of charge injection from the electrode(s) or by the ability of the dielectric to transport injected charges. These two transport modes can be visualized by considering a gardener who is watering his flowers using a hose attached to a tap. If he opens the tap just a little bit, the water flow is limited by the opening of the tap. However, when gradually opening the tap further there will be a point at which it does not matter how wide the gardener opens the tap because the water flow becomes entirely coordinated by the flow resistance of the hose. In an electrically addressed diode, the former case is referred to as *injection-limited current*; in the latter case, it is called a *space-charge-limited (SCL) current.*

In either case, the current density through the device is given by the number N of charges e that flow per unit time t and unit area A,

$$j = \frac{eN}{At} = \frac{eN}{At}\frac{l}{l} = env = en\mu F \tag{3.1}$$

where $n = N/Al$ is the number density of charges, l is a unit length, $v = l/t$ is the mean drift velocity that charges in a device obtain under the influence of an electric field F. $\mu = v/F$ is the associated mobility of the charges. A closely related quantity is the *diffusivity D*, also synonymously called *diffusion constant D* or *diffusion coefficient D* . It is defined by $\boldsymbol{j} = -eD\boldsymbol{\Delta}n$, where D is a tensor. In one dimension, this reduces to $j = -eD\,\partial n/\partial x$, with D being a scaler. The diffusion coefficient has the the SI units m^2s^{-1}. The diffusivity yields the mean distance that a diffusing particle travels within a time t as $l = \sqrt{Dt}$ (Box 3.1).

Box 3.1 Isotropic Diffusion

In the absence of an external gradient, for example, due to electric field, temperature or concentration, the diffusion of a charge or an excitation can be treated as a random walk. The basic idea is that the moving particle executes a series of on average equidistant steps, in on average equal time intervals. The direction of each step is taken at random, and it is independent of the previous step. After a time t, the particle is at a distance l from its starting point, though the actual path traveled may be significantly longer (Figure B3.1.1). One can show [1, 2] that the distance covered

Samsung Exhibit 1058, Page 15 of 33
Samsung v. W&Wsens - PGR2025-00082

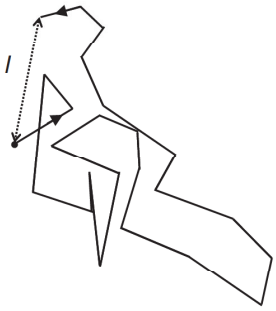


Figure B3.1.1 Schematic illustrating the random walk of an exciton. The final distance *l* from the starting point is much less than the overall distance traveled.

increases as the square root of time, more precisely

$$l = \sqrt{ZDt} \tag{B3.1.1}$$

with $Z = 6,4,2$ for three-dimensional, two-dimensional, and one-dimensional diffusion, respectively. The proportionality factor D is the diffusion constant (synonymously referred to as *diffusion coefficient*), typically given in units of square centimeter per second. Values reported in the literature for D vary by roughly a factor of 2 due to the inconsistency in the Z-values chosen [3]. Often, Z is taken to be unity, for example, if one associates l with the exciton diffusion length l_d and t with the exciton lifetime τ, so that $l_d = \sqrt{D\tau}$. The three-dimensional diffusion constant is usually expressed as $D = (1/6)a^2\nu_h$, which follows from Eq. (B3.1.1) if one takes l as the hopping distance a to the next site, and t corresponds to the jump time, which is the inverse of the hopping frequency ν_h.

3.1.1
Injection Limited Currents

An injection limited current reflects only the mechanism by which charge carriers are injected and not their subsequent transport. This is easily seen when considering the rate equation for, say, holes, that are generated at the anode and that decay either in a monomolecular fashion through discharge at the cathode or by bimolecular recombination with electrons injected from the cathode. The associated rate equation is

$$\frac{dn_+}{dt} = G - k_{tr}n_+ - \gamma n_- n_+ \tag{3.2}$$

Here G is the rate of hole injection per unit volume and n_+ and n_- are the hole and electron concentrations. k_{tr} is the rate constant for monomolecular decay. $k_{tr} = 1/\tau_+$ corresponds to the reciprocal transit time for a hole in a diode with thickness d under the action of an applied field F, $\tau_+ = d/\mu_+F$, where μ_+ is the hole mobility. γ is the rate constant for bimolecular recombination.

If electron injection from the cathode is small compared to the hole injection from the anode, so that $\gamma n_+ n_- \ll n_+ k_{tr}$, the steady state condition $dn_+/dt = 0$ implies that $n_+ = G/k_{tr}$. Inserting this into the equation for current, Eq. (3.1), yields

$$j = e\frac{G}{k_{tr}}\mu_+F = e\frac{G}{\mu_+F}d\mu_+F = eGd = eg \tag{3.3}$$

where $g = Gd$ is the injection rate per unit area. Equation (3.3) highlights the fact that the current is controlled only by the injection rate. Any dependence of the current on the electric field and temperature is therefore a reflection of the injection process and does not yield any information on the charge carrier mobility. This is an important insight to keep in mind for the case of injection limited current. The above consideration can, of course, be extended to the case of injection from both electrodes.

Samsung Exhibit 1058, Page 16 of 33
Samsung v. W&Wsens - PGR2025-00082

3.1.2 Unipolar Space Charge Limited (SCL) Current

When the supply of charge carriers injected from the electrode(s) is unlimited, the current will eventually be limited by its own space charge that shields the electric field at the injection electrode. An electrode that is able to inject more charges than can be transported through the device is conventionally called an *ohmic electrode*. The term *ohmic* may be confusing because it may invoke the allusion of Ohm's law that predicts a current that varies linearly with the electric field. However, an SCL current injected from an ohmic electrode does *not* obey Ohm's law. A simple calculation shows this. Consider an OLED as a simple metal–insulator–metal-type structure. In such a sandwich-type capacitor with thickness d, capacitance per unit area C, and a dielectric relative permittivity ε_r, the capacitor charge per unit area is $q = CV = \varepsilon_r\varepsilon_0 V/d$. If all capacitor charges will migrate toward the exit electrode, the resulting current per unit area is $j = q/\tau_{transit}$. The time the charges need to traverse the diode, that is, the transit time, is $\tau_{transit} = d/\mu F = d^2/\mu V$. This yields $j = \varepsilon_r\varepsilon_0\mu F^2/d$. This is the maximum unipolar current that can flow through the device. In this simplified calculation, we tacitly assumed that the electric field in the dielectric is spatially homogeneous. This is not true. It turns out, however, that the correct expression, which is referred to as *Child's law for unipolar SCL current flow*, or also the *Mott–Gurney equation*, is

$$j = \frac{9}{8}\varepsilon_r\varepsilon_0\mu\frac{F^2}{d} = \frac{9}{8}\varepsilon_r\varepsilon_0\mu\frac{V^2}{d^3} \tag{3.4}$$

It deviates from the above approximate equation by only 11%. Note that in Eq. (3.4), the voltage refers to the voltage applied to the device corrected for the built-in voltage, that is, $V = V_{applied} - V_{built\text{-}in}$. A rigorous derivation of Child's law requires solving *Poisson's equation*

$$\frac{\mathrm{d}F}{\mathrm{d}x} = \frac{ne}{\varepsilon_r\varepsilon_0} \tag{3.5}$$

the *continuity equation,*

$$j = en\mu F - De\frac{\mathrm{d}n}{\mathrm{d}x} \tag{3.6}$$

and the *Einstein relation* between diffusivity D and mobility μ,

$$eD = \mu kT \tag{3.7}$$

For the condition of low electric field, the validity of the Einstein relation in disordered organic semiconductors has been confirmed [4]. For the detailed derivation of Child's law, we refer the reader to textbooks such as [3, 5]. We only mention important elements and results of the theory:

(i) Equation (3.4) implies that at a given electric field, the SCL current scales inversely with the device thickness. This thickness dependence is the crucial criteria to decide whether a superlinear current field dependence of the current is caused either by space charge limitation or by field dependent charge carrier injection [6]. Fitting a current–voltage dependence with Child's law, Eq. (3.4), when the thickness dependence criterion actually indicates injection-limited current leads to erroneous values for the mobility that reflect the field dependence of the injection process, as already mentioned above.

(ii) The electric field inside the dielectric varies as

$$F(x) = \frac{3}{2}\frac{V}{d}\sqrt{\frac{x}{d}} \tag{3.8}$$

where x is counted from the injecting electrode. The field is zero at an (ohmic) electrode and it is $(3/2)(V/d)$ at the exit electrode. The charge concentration also depends on the spatial coordinate and is given by

$$n(x) = \frac{3\varepsilon_r\varepsilon_0 V}{4ed^2}\sqrt{\frac{d}{x}} \tag{3.9}$$

Samsung Exhibit 1058, Page 17 of 33
Samsung v. W&Wsens - PGR2025-00082

The average concentration is

$$n = \frac{3}{2}\varepsilon_r\varepsilon_0\frac{V}{ed^2} \tag{3.10}$$

that is, 3/2 times the number of capacitor charges per unit volume.

(iii) Equation (3.4) is strictly valid only if the charge carrier mobility is field-independent because a field dependence of μ would have a feedback on the spatial distribution of the space charge. This would cause a deviation from Child's law. Young [7] treated this problem and showed that there is no explicit solution for an arbitrary field dependence of μ. For this reason, it would be incorrect to calculate a field-dependent mobility presuming the validity of Eq. (3.4). In fact, it has meanwhile been recognized that such a deviation from Eq. (3.4) is caused by filling up deep states of the DOS (density of states) distribution of the intrinsic hopping sites.

If an electrode cannot supply sufficient charge carriers to maintain SCL conditions, the current is injection limited, that is, it is determined by the number of charge carriers an electrode is able to inject. Whether or not an electrode is able to sustain an SCL current depends on both the injection barrier and on the charge carrier mobility of the dielectric, that is, the organic semiconductor. For ideal interfaces, the injection barrier is given by the energy difference between the workfunction of the electrode and the ionization potential or electron affinity of the organic semiconductor (Figure 3.2a). (As discussed in Sections 1.3.3 and 2.4.4, for visualization purposes, the ionization potential and electron affinity are often approximated as HOMO and LUMO in a one-electron picture [8].) Obviously,

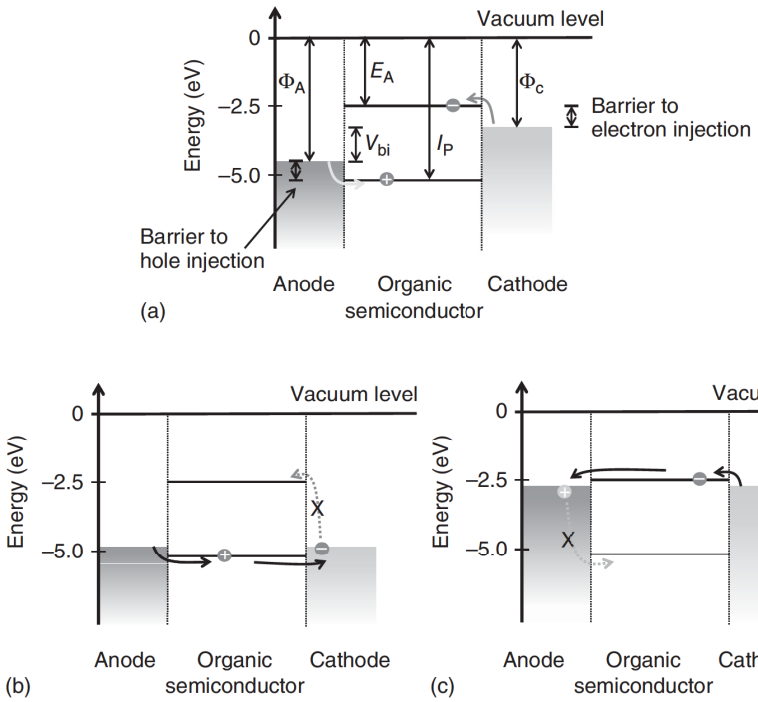


Figure 3.2 Energy level for an organic semiconductor diode. (a) A common alignment of energy levels for OLED or OSC function. The work functions Φ_A and Φ_C of anode and cathode as well as the electron affinity E_A and ionization potential I_P of the organic semiconductor are indicated. The energy barriers to injection as well as the magnitude of the built-in potential V_{bi} are also shown. (b) The alignment of electrode workfuntions for a hole-only device. The high barrier at the cathode prevents electrode injection. (c) The alignment of electrode workfuntions for an electron-only device.

Samsung Exhibit 1058, Page 18 of 33
Samsung v. W&Wsens - PGR2025-00082

the higher the mobility, the more crucial is the height of the injection barrier. As a rough estimate for a conjugated polymer with average mobility, say, $10^{-4}\,\mathrm{cm^{-2}\,V^{-1}\,s^{-1}}$, a tolerable barrier is 0.3 eV [9]. Thus, when using PEDOT:PPS as a hole injecting electrode with a maximum workfunction of −5.1 eV, ohmic injection and associated SCL current prevail when the HOMO level of the transport material is no lower than −5.4 eV at most.

A complication arises if the dielectric contains traps. In that case, the mobility that enters in Eq. (3.4) represents an effective mobility that is determined by the trap concentration and their energetic depth that controls thermally activated detrapping. This effective mobility can be determined experimentally (see Section 3.3). If the traps are mono-energetic, the functional form of Child's law is retained. However, in disordered materials, this is the exception rather than the rule. Even in molecular crystals, traps are usually distributed in energy. This causes a deviation from the analytic form of Child's law. This is easy to understand but difficult to assess quantitatively. Consider a distribution of trap levels. When applying an electric field to a diode with an ohmic injecting electrode and a non-injecting counter electrode, the charge carriers tend to fill up the trap states starting energetically from the bottom. Therefore, the activation energy needed for detrapping the charge carriers decreases with increasing field and, concomitantly, the $j(F)$ dependence must become steeper than Child law would predict. Mark and Helfrich [10] solved this problem analytically for the case of an exponential trap density distribution of the form

$$n(E_t) = \frac{N_t}{kT_c}\exp\left(-\frac{E_t}{kT_c}\right), \quad \text{with} \quad \frac{T_c}{T} = l > 1 \tag{3.11}$$

where T_c is a measure of the steepness of the distribution and N_t is the total density of traps. E_t is the energetic depth of the trap, that is, the energy difference between the energy level of the trap and the electron affinity (for electron traps) or ionization potential (for hole traps). For such an exponential trap distribution one finds

$$j(V) \propto \frac{V^{l+1}}{d^{2l+1}} \tag{3.12}$$

For a Gaussian trap distribution, an exact analytic solution for the SCL current does not exist, so that the Poisson equation and the continuity equations would need be evaluated numerically [11, 12]. However, Nicolai *et al.* [13] showed that the effects of a Gaussian trap distribution can be incorporated into an analytical, approximative solution by introducing an effective trap depth that depends on the width of the trap distribution. By analyzing the field and temperature dependences of the SCL current one can extract the relevant parameters such as the trap depth, the density of trap states, and the Gaussian width of the trap distribution [12]. Note that the SCL current is then not linear on a $\log j$ versus $\log V$ plot. This is a specific feature of a Gaussian trap distribution.

Figure 3.3 illustrates how Child's law applies to a diode made with dialkoxy-substituted PPV. Figure 3.3a shows the current–voltage curves obtained for dialkoxy films of different thicknesses, using indium–tin-oxide (ITO) and gold as electrodes. The energy levels of both electrodes are unsuitable for electron injection into the LUMO of the dialkoxy-PPV, so that only charge transport via the HOMOs is measured (Figure 3.2b). Thus, the ITO/PPV/Au structure results in a *hole-only device* that allows for measuring the hole current without contributions from an electron current. The solid lines in Figure 3.3a are fits using the equation for trap-free *SCL*, current, Eq. (3.4). Clearly, agreement with the experimental data is excellent. It demonstrates that the hole current is SCL and not injection-limited. Using $\varepsilon_r = 3$ yields a hole mobility of $0.5 \times 10^{-6}\,\mathrm{cm^2\,V^{-1}\,s^{-1}}$. The transport properties of electrons in the LUMO are investigated for an *electron-only device* made by sandwiching the dialkoxy-PPV between two Ca electrodes. The workfunction of Ca is close to the LUMO of the dialkoxy-PPV resulting in efficient electron injection into the LUMO, yet with negligible hole injection into the HOMO (Figure 3.2c). The resulting current–voltage curves are shown in Figure 3.3b. A much steeper dependence of current on voltage is evident for the electron current than for the hole current in Figure 3.3a. The data can be fitted approximately using the equation for trap-limited SCL current, assuming an exponential trap distribution, Eq. (3.12). The analysis of

Samsung Exhibit 1058, Page 19 of 33
Samsung v. W&Wsens - PGR2025-00082

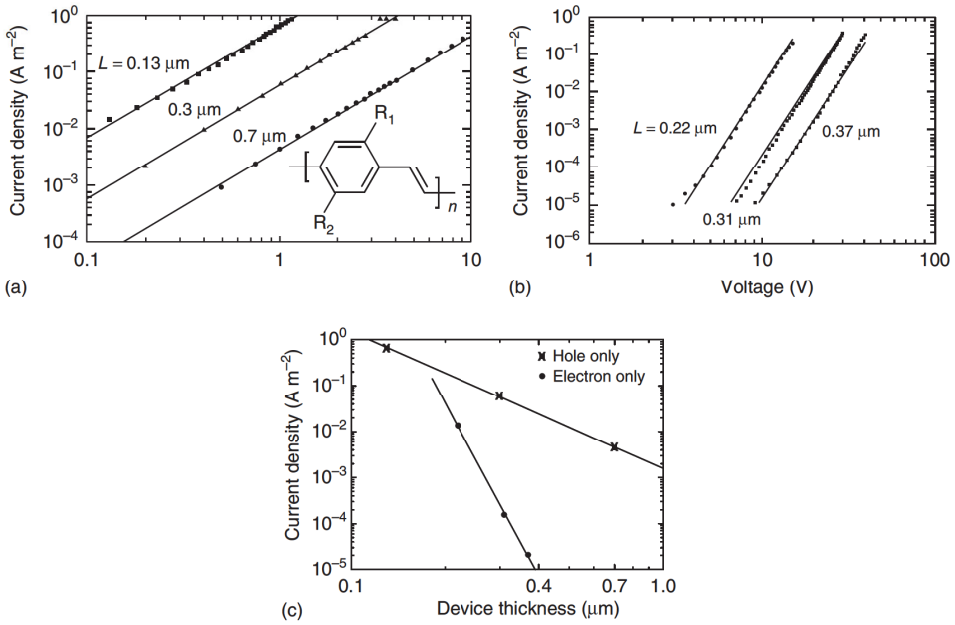


Figure 3.3 (a) Current–voltage curves for hole-only devices made in a sandwich structure of ITO/dialkoxy-PPV/Au with film thicknesses of $L = 0.13$, 0.30, and 0.7 µm. Symbols indicate the experimental data, and solid lines are fits according to Eq. (3.4), showing a clear $j \propto V^2$ dependence. The inset shows the PPV used with $R_1 = CH_3$ and $R_2 = C_{10}H_{21}$. (Data from Blom *et al*. [6].) (b) Current–voltage curve for an electron-only device made in a sandwich structure of Ca/dialkoxy-PPV/Ca with film thicknesses of $L = 0.22$, 0.31, and 0.37 µm. Symbols indicate the experimental data, and solid lines are fits according to Eq. (3.12). (c) Hole-only and electron-only current densities in dialkoxy-PPV diodes as a function of the film thickness. Hole-only current and electron-only currents were measured at a bias voltages of 1 and 10 V, respectively. (Data from Blom *et al*. [6].)

the current–voltage curve in terms of an SCL current can be further justified by considering the thickness dependence. Figure 3.3c shows the much steeper thickness dependence found for the data pertaining to the electron current as compared to the data for the hole current. In both cases, the predicted dependences, $j(V) \propto d^{-3}$ and $(V) \propto d^{-2l-1}$, are obeyed.

If the concentration of the charge carriers stored in the diode exceeds the number of traps, there is a transition from trap-limited SCL transport to trap-free transport. The signature of this effect of "trap-filling" is an abrupt increase of the SCL current. This occurs at the field F_{TFL} where the trap concentration N_t is

$$N_t = \frac{\varepsilon_r \varepsilon_0}{ed} F_{\mathrm{TFL}} \tag{3.13}$$

For a 150 nm thick diode containing 4×10^{16} cm^{-3} traps the critical applied voltage (field) for trap filling is about 5 V (3.2×10^4 V cm^{-1}).

As mentioned before, care must be taken when assigning a super-linear $j(F)$ characteristic with SCL current flow. An unambiguous distinction between a super-linear injection limited current and an SCL current is provided by the thickness dependence at a given electric field. Note that Eq. (3.12) predicts an even stronger thickness dependence of a trapping controlled SCL current as compared to Child's law.

Samsung Exhibit 1058, Page 20 of 33
Samsung v. W&Wsens - PGR2025-00082

3.1.3 Bipolar Space Charge Limited Current

The formalism to describe a unipolar SCL current can be extended to the case of injection from both electrodes. Consider the case where both anode and cathode are ohmic and positive and negative space charges are injected from opposite electrodes. If these charges meet somewhere in the bulk of the organic semiconductor and recombine with unit probability, one can show [14, 15] that the total current results from the superposition of the positive and negative SCL currents, that is,

$$j = \frac{9}{8}\varepsilon_r\varepsilon_0(\mu_+ + \mu_-)\frac{V^2}{d^3} \tag{3.14}$$

A key element in the derivation is that the charges recombine in the bulk with very high probability. To show this, we consider a majority hole current injected from an anode, $j = en_+\mu_+F$, and a single electron injected from the cathode. The latter can either traverse the diode and arrive at the cathode after the transit time $\tau_{transit} = d/\mu_-F$, or it can recombine with one of the holes whose concentration is $n_+ = j/e\mu_+F$. In the former case of the electron reaching the anode, the hole density at the anode would be reduced and the space-charge-limitation of the current from the anode would no longer be granted. To assess how likely this is, we shall calculate the probability p_- for the electron to recombine with a hole instead of reaching the anode. The probability for the electron to arrive at the anode is then 1- p_-. Consider the rate equation for the electron current. Analogous to Eq. 3.2, it is given by $\frac{dn_-}{dt} = G - k_{tr}n_- - \gamma n_+ n_-$. This contains the term $k_{tr}n_-$ due to charge carrier drift and the recombination term $\gamma n_+ n_-$. Evidently, the rate of recombination is γn_+. The probability that the electron will recombine with a hole is given by the recombination rate over the sum of all decay rates, i.e.

$$p_- = \frac{\gamma n_+}{\gamma n_+ + \tau_{transit}^{-1}} = \frac{1}{1 + \frac{\mu_- F}{d\gamma n_+}} \tag{3.15}$$

Let us evaluate the recombination coefficient γ. In general, the bimolecular recombination coefficient γ is given by the *Smoluchowski recombination rate*,

$$\gamma = 4\pi R_{AB}(D_A + D_B) \tag{3.16}$$

where D_A and D_B are the diffusion constants of reactants A and B, and R_{AB} is the separation at which the reaction takes place. If the reactants are charges, as is the case here, their diffusion coefficients are related to the mobility through the Einstein relation Eq. (3.7). R_{AB} is the Coulomb capture radius,

$$R_{AB} = \frac{e^2}{4\pi\varepsilon_r\varepsilon_0 kT} \tag{3.17}$$

The Coulomb capture radius gives the distance where the thermal energy of two opposite charges is equal to their attractive Coulomb energy, that is, $kT = e^2/4\pi\varepsilon_r\varepsilon_0 R_{AB}$. Inserting Eqs. (3.7) and (3.17) into Eq. (3.16) gives

$$\gamma = \frac{e}{\varepsilon_r\varepsilon_0}(\mu_+ + \mu_-) \tag{3.18}$$

If we use this in Eq. (3.15), we obtain

$$p_- = \frac{1}{1 + (\mu_-/(\mu_+ + \mu_-))(\varepsilon_r\varepsilon_0 F/edn_+)} \tag{3.19}$$

In the case where the hole current is SCL, we can use Eq. (3.10), that is, $n_+ = 1.5\varepsilon_r\varepsilon_0 F/de$. Inserting this into Eq. (3.19) yields

$$p_- = \frac{1}{1 + (2/3)(\mu_-/(\mu_+ + \mu_-))} \tag{3.20}$$

Samsung Exhibit 1058, Page 21 of 33
Samsung v. W&Wsens - PGR2025-00082

We can evaluate Eq. (3.20) for different ratios between the electron and hole mobility. If $\mu_- \ll \mu_+$, we have $\mu_-/(\mu_+ + \mu_-) \ll 1$, so that $p_- \to 1$. If $\mu_- = \mu_+$, $\mu_-/(\mu_+ + \mu_-) = 1/2$ and $p_- = (3/4) = 0.75$. If $\mu_- \gg \mu_+$, we obtain $\mu_-/(\mu_+ + \mu_-) \approx 1$ leading to $p_- \approx (3/5) = 0.6$.

This simplified calculation indicates a high probability for the electron to recombine instead of traversing to the anode. This calculation gives, however, only a lower bound for the recombination yield because it ignores the fact that in case of SCL current flow, the electric field is not constant but becomes zero at the ohmic electrode (see Eq. (3.8)). Therefore, the electron that we have considered will finally enter a region of vanishing electric field. There, its motion will ultimately become diffusive so that it will not reach the anode but will recombine with a hole next to the anode with certainty. Thus, the premise that injection from two ohmic electrodes leads to near unity recombination is supported, and the total current can be described by superimposing two SCL currents as expressed in Eq. (3.14).

For a rigorous treatment of this phenomenon, the reader is referred to the original seminal works [14, 15]. However, even the above simple calculation leads to important conclusions:

- First, an ohmic electrode maintains to be ohmic (in the sense of supporting a SCL current) even when the counter-electrode is also ohmic. The individual currents are SCL and controlled by the mobilities of electron and hole. If $\mu_+ = \mu_-$, most of the recombination events will occur in the middle of the diode. Otherwise, the recombination zone shifts toward that electrode from where the less mobile charge carriers are injected, so that recombination occurs at $x_m = d/((\mu_-/\mu_+) + 1)$, where x_m is the distance from the anode and d is the thickness of the organic layer.
- Second, electrons and holes injected from electrodes that are both ohmic recombine with unit probability. On the other hand, when the current is injection limited many of the charge carriers get discharged at the electrodes instead of recombining. This follows from Eqs. (3.15) and (3.19), since the charge carrier densities n_+ and n_- are, by definition, lower for an injected limited current than for an SCL current. The fabrication of OLEDs with optimized luminescence yield therefore requires that both electrodes are able to deliver SCL currents.

The conclusion that electrons and holes in an OLED with two ohmic electrodes will recombine with certainty rests upon the notion of Langevin-type recombination (see Section 3.4). If the recombination is less strong, an overall neutral combination of electron and hole densities is established in which excess charges can traverse the diode without suffering bimolecular recombination. Whether or not this case is realized can be estimated by comparing the total diode current with the sum of the individual SCL electron and hole currents injected from the respective electron-only and hole-only devices [16].

3.2 Charge Injection Mechanisms

Undoped organic semiconductors are, in fact, insulators unless charge carriers are injected from the electrodes or generated in the bulk by optical excitation (Box 3.2). To proof this statement, one can adopt the classic semiconductor theory to estimate the concentration of charge carriers existing in the dark in a semiconductor under equilibrium conditions. Since the electrical gap between hole and electron transporting states is usually at least 2 eV, (e.g., for the π-conjugated polymer poly(3-hexylthiophene) (P3HT), the electrical gap is 2.6 eV [17]) and the Coulomb attraction between positive and negative excess charge is poorly screened, the intrinsic concentration of free carriers is negligible. The charge carriers needed for the successful operation of an OLED and OFET have to be injected. The crucial parameter for this is the energy difference between the work function of the electrode and the hole or electron transporting states. This barrier can be overcome by either tunneling or thermal activation.

Samsung Exhibit 1058, Page 22 of 33
Samsung v. W&Wsens - PGR2025-00082

Box 3.2 Conductivity of a Semiconductor

The difference between a semiconductor and an insulator is best assessed by considering the conductivity σ_c of the material [18]. It is the product of the elementary charge e, the mobility μ of charge carriers, and their concentration n, that is, $\sigma_c = en\mu$. In traditional semiconductors such as silicon, germanium, or Ga_2As_3, the conductivity is between, say, 10^{-8} and $10^{-2}\ \Omega^{-1}\ cm^{-1}$. In an undoped solid, the concentration of free charge carriers is determined by $n = N_{eff}e^{-E_g/2kT}$ where N_{eff} is the effective density of valence or conduction band states and E_g is the band gap. For crystalline silicon, E_g is 1.1 eV and the charge carrier mobility is about $1000\ cm^2\ V^{-1}\ s^{-1}$. This predicts an intrinsic conductivity of about $10^{-6}\ \Omega^{-1}\ cm^{-1}$ at room temperature. Note that a band gap of 1.1 eV translates into an absorption edge of 1100 nm. In view of the relative dielectric constant as large as $\varepsilon_r = 11$, Coulomb-effects between electrons and holes are unimportant and electrons and holes are essentially free at room temperature. This implies that optical absorption is due to a transition from valence band to a conduction band. The situation is fundamentally different in undoped molecular solids. Their absorption edge is usually larger than 2 eV and the dielectric constant is 3–4. In this case, optical absorption generates Coulomb-bound electron–hole pairs with a binding energy of 0.5–1.0 eV. Even if one were to ignore the exciton binding energy and to identify incorrectly the optical absorption edge with a valence to conduction band transition, the resultant intrinsic conductivity would be much less than $10^{-12}\ \Omega^{-1}\ cm^{-1}$, assuming a charge carrier mobility of $1\ cm^2\ V^{-1}\ s^{-1}$, that is, the materials are insulators. However, they can become semiconducting if charge carriers are generated extrinsically.

3.2.1 Fowler–Nordheim Tunneling Injection

Originally, this formalism was introduced to explain the electron emission from a metallic tip into vacuum, for example, when explaining the operation of a scanning transmission microscope (STM). The injection barrier is identified with the workfunction of the metal, ϕ. Upon applying a strong electric field, electrons can tunnel from the Fermi level of the metal through a triangular barrier into the vacuum. The triangular barrier is determined by the superposition of the rectangular barrier due to the metal–vacuum interface and the applied potential (Figure 3.4). Fowler and Nordheim [19] predicted that the injection current depends on the applied electric field as

$$j_{NF}(F) \cong F^2 \exp\left(-\frac{4\sqrt{2m_{eff}\phi^3}}{3\hbar eF}\right) \tag{3.21}$$

that is, a plot of $\ln(j_{NF}/F^2)$ versus $1/F$ should yield a straight line with a slope proportional to $\phi^{3/2}$. Applying this concept to an organic diode causes serious problems.

First, in Eq. (3.21), the image potential (see below) is ignored. This is justified in the case of injection into vacuum where the injection barrier is much higher than an image charge (see below), yet not for a diode in which the injection barrier is lowered by the electron affinity of the diode material.

Second, for a 100 nm thick diode and an applied voltage of 5 V, the electric field is $5 \times 10^5\ V\ cm^{-1}$. Even assuming an injection barrier as low as 0.5 V, the distance an electron had to tunnel without suffering inelastic scattering is 10 nm, that is, 10 times the intermolecular spacing. This is unrealistic for a disordered molecular semiconductor, and even for molecular crystals at room temperature. For these reasons one can ignore Fowler–Nordheim tunneling as the main source of injection in a sandwich type OLED. This process can only become important in a diode with rough electrode surfaces where high electric field can exist at local tips. They can promote injection always at the same spot and may eventually cause breakdown of the diode.

Samsung Exhibit 1058, Page 23 of 33
Samsung v. W&Wsens - PGR2025-00082

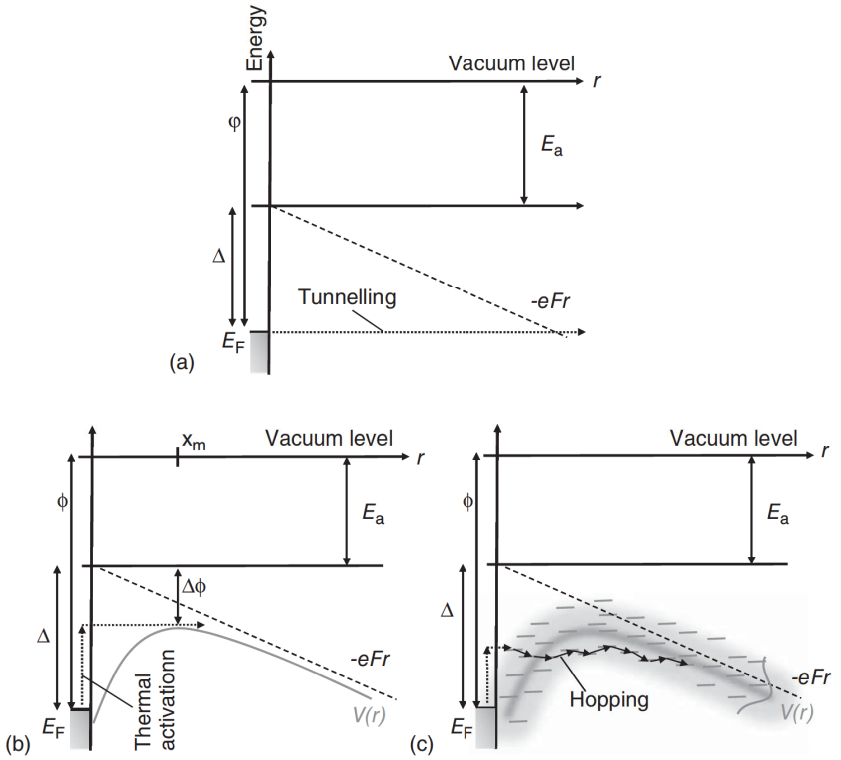


Figure 3.4 Schematic representation of electron injection from a metallic electrode into a semiconductor (a) via Fowler–Nordheim tunneling, (b) via Schottky emission, and (c) via hopping in a disordered organic solid. *r* denotes the distance from the electrode. The dashed line indicates the potential energy due to the applied (external) electric field *F*. The potential *V*(*r*) in the device is shown as a gray solid line. Note the reduced activation energy and tunneling distance in (c) compared to (b). Note the reduced activation energy and tunneling distance in (c) compared to (b).

3.2.2
Richardson–Schottky Thermionic Injection

Consider the injection of an electron that is thermally excited from the Fermi level of a planar metallic electrode with workfunction ϕ to a semiconductor with an electron affinity E_a. Frequently, $|E_a| < |\phi|$, so that there is a potential barrier $\Delta = \phi - E_a$ from the metal to the semiconductor. The idea behind Richardson–Schottky type injection is that the electron induces an image charge at an equal distance from the interface to that of the real charge (Figure 3.4). The total potential $V(x)$ experienced by the electron is then composed of the potential barrier $\Delta = \phi - E_a$, the image potential $\phi_{image} = -e^2/16\pi\varepsilon_0\varepsilon_r x$, and the applied electrostatic potential eFx. It is

$$V(x) = (\phi - E_a) - \frac{e^2}{16\pi\varepsilon_0\varepsilon_r x} - eFx \tag{3.22}$$

ϕ_{image} is derived by considering the Coulomb force K acting between a charge e located at a distance x from the electrode and its image charge $-e$ at a distance $-x$ from the interface,

$$K = -\frac{e^2}{4\pi\varepsilon_0\varepsilon_r(2x)^2} \tag{3.23}$$

Samsung Exhibit 1058, Page 24 of 33
Samsung v. W&Wsens - PGR2025-00082

The work done to an electron that is transferred from infinity to x is given by

$$\int_{\infty}^{x} K\mathrm{d}x = -\frac{e^2}{16\pi\varepsilon_0\varepsilon_r x} \tag{3.24}$$

This energy corresponds to the potential energy of an electron that is placed at a distance x from the interface. The distance from the electrode where the maximum of the total potential occurs can be calculated from $\mathrm{d}V(x)/\mathrm{d}x = 0$. Importantly, the maximum is not located at the interface but rather at the distance

$$x_m = \sqrt{\frac{e}{16\pi\varepsilon_0\varepsilon_r F}} \tag{3.25}$$

At x_m, the injection barrier is lowered by

$$\Delta\phi = \sqrt{\frac{eF}{4\pi\varepsilon_0\varepsilon_r}}e \tag{3.26}$$

The injection current is predicted to be

$$j_{RS} \propto T^2 \exp\left(-\frac{\Delta - \Delta\phi}{kT}\right) = T^2 \exp\left(-\frac{\phi - E_a - \beta_{RS}\sqrt{F}}{kT}\right) \tag{3.27}$$

with $\beta_{RS} = \sqrt{e^3/4\pi\varepsilon_0\varepsilon_r}$. Equation (3.27) predicts

$$\ln(j_{RN}(F)) \propto \sqrt{F} \tag{3.28}$$

This type of field dependence is characteristic for a process in which a charge is transferred across a Coulomb potential superimposed onto an applied potential regardless if the Coulomb potential is created by a real charge or by an image charge. In the former case, it is termed *Poole–Frenkel*-type field dependence, considering, though, that the numerical prefactor β in the exponent is specific for a particular kind of process i.e., $\beta_{PF} = \sqrt{e^3/\pi\varepsilon_0\varepsilon_r}$ for a Poole-Frenkel process yet $\beta_{RS} = \sqrt{e^3/4\pi\varepsilon_0\varepsilon_r}$ for the Richardson-Schottky injection.

The Richardson–Schottky concept is premised upon the notion that once an electron has acquired enough thermal energy to overcome the potential barrier, it traverses the potential barrier in field direction without suffering inelastic scattering. Otherwise, the electron would recombine with the image charge and be lost for the injection process. Whether or not this condition is satisfied depends on the electric field and the scattering length of the charge carriers. For a representative value of $2\times10^5\,\mathrm{V\,cm^{-1}}$ for the electric field and $\varepsilon_r = 3$, the potential maximum is about 2.5 nm away from the interface, that is, about 2.5 times the intermolecular spacing. Therefore, one cannot expect that a thermally activated injection current obeys strictly the Richardson–Schottky model.

3.2.3
Thermally Activated Injection into a Disordered Organic Semiconductor

The injection models described by either Fowler–Nordheim tunneling or Richardson–Schottky thermionic emission were originally devised with a view to crystalline, inorganic semiconductors. Based upon the simulation and analytic theory [20], a model has meanwhile been developed that takes into account (i) the existence of the image charge at the electrode, (ii) the hopping-type of charge transport, and (iii) the presence of disorder existing in a noncrystalline system. It is illustrated in Figure 3.4. The underlying idea, originally introduced by Gartstein and Conwell [21] is that a thermally activated jump raises an electron from the Fermi level of the electrode to a tail state of the density of states (DOS) distribution of transport sites of the dielectric medium. This is subject to the condition that this site has at least one neighboring hopping site at equal or even a lower energy. It is fulfilled by optimizing a transport parameter with regard to both jump distance and

Samsung Exhibit 1058, Page 25 of 33
Samsung v. W&Wsens - PGR2025-00082

jump energy. This condition ensures that the primarily injected carrier can continue its motion away from the interface rather than recombine with its image charge in the electrode. Subsequently, the carrier is considered to execute a diffusive random walk in the combined Coulomb potential of the image charge and the externally applied potential. Simulation and analytic theory for injection barriers ranging from 0.2 to 0.7 eV and temperatures between 300 and 200 K are mutually consistent. Apparently, the neglect of the stochastic nature of the carrier motion in the vicinity of the electrode as well as the neglect of disorder on the one-dimensional Onsager-type escape process (see Section 3.6.2) is uncritical in the considered parameter regime. The field dependence of the injection efficiency follows a Poole–Frenkel – type of field dependence (see Eq. (3.28)).

However, when plotting an injection current on a $\ln j$ versus $1/T$ scale, as one does when analyzing the temperature dependence of a conventionally activated process (Box 3.3), one finds that the apparent activation energy obtained from the slope of the $\ln j$ versus $1/T$ dependence is much less than the one which one would expect based upon presumed injection barriers, taken from literature values of the workfunction of the electrode and the electron affinity/ionization energy of the dielectric. The explanation of this ubiquitously observed phenomenon is related to the stochastic motion of charges in a rough energy landscape that will be described in Section 3.3.2. It rests on the concept of the transport energy at which charge carriers, on average, migrate within a given DOS distribution. This transport energy decreases when the temperature decreases and, thus, the energy to overcome the injection barrier is no longer constant but decreases with temperature (see Section 3.3.2). As a consequence, the slope of the measured $\ln j$ versus $1/T$ dependence is not a direct measure of the injection barrier. The actual injection barrier has to be inferred from the formalism laid down in Ref. [20].

Box 3.3 Arrhenius Plot

By the laws of statistics, the rate w of a thermally activated process depends exponentially on the required activation energy E_a, that is, $w(T) = w_0 \exp(-E_a/kT)$. It is convenient to plot the rate logarithmically as a function of inverse temperature, that is, $\ln w(T) = -(E_a/k)(1/T) + \ln w_0$. Such a representation is called an *Arrhenius plot*. From comparison with $y = mx + c$, it is evident that the activation energy can easily be read off the plot by multiplying the slope with the Boltzmann-constant k.

Woudenbergh *et al.* [22] applied the Arkhipov *et al.* formalism to explain injection limited hole currents in π-conjugated polymers. Agrawal *et al.* [23] compared injection-limited currents and SCL currents in a copper-phthalocyanine sandwich cell with ITO and Al electrodes. An analysis of experimental data yields consistent values for the width of the DOS distribution as well as for inter-site separation. These studies support the model of thermally activated injection into a Gaussian DOS distribution of hopping sites and confirm the notion that disorder facilitates injection because it lowers the injection barrier although the transport velocity decreases with increasing disorder. We shall elaborate on this problem in greater detail by including experimental results from the work of Mihailetchi *et al.* [24] who used a PCBM diode sandwiched between an ITO/PEDOT:PPS electrode and an either gold or silver counter-electrode as a test system for electron injection. Those data show how a technically simple study of conductivity can be employed for determining both the actual injection barrier as well as the actual workfunction of the metal electrode. The workfunction of the PEDOT:PSS anode in that diode is 5.2 eV, and the literature values for the workfunctions of gold and silver are 5.1 and 4.4 eV [25]. Since the ionization potential and electron affinity of PCBM are at −6.1 and −3.7 eV [24], respectively, the energy barriers for both electron and hole injection should be on the order of 1 eV (Figure 3.2). Therefore, the current flowing through the diode is presumed to be injection limited. As portrayed in more detail in Chapter 4, when applying an external voltage V to a diode with different workfunctions $\phi_{cathode}$ and ϕ_{anode}, one has to take into account that there is a built-in potential V_{bi} so that the voltage acting on the dielectric is reduced by the built-in

Samsung Exhibit 1058, Page 26 of 33
Samsung v. W&Wsens - PGR2025-00082

potential to $V - V_{bi}$. In diode structures where the energy barrier for injection is sufficiently large, that is, ≥0.6 eV, the equilibrium density of thermally injected charge carriers is negligible [26], and the diode can be treated as a metal–insulator–metal structure. V_{bi} is then simply given by the difference between the workfunctions of the electrodes, that is, $V_{bi} = \phi_{anode} - \phi_{cathode}$. Note that this is no longer granted when the injection barrier is smaller, notably when one or both electrodes are ohmic. V_{bi} can be determined from the current–voltage curve measured under photoexcitation. If the applied voltage is smaller than V_{bi}, the electric field in the film is such that electrons drift to the cathode and holes to the anode. For $V > V_{bi}$, the direction of current flow is reversed (cf. Section 4.1.3, Figure 4.6). The abscissa intercept of the current therefore defines V_{bi}. In this way, a value for V_{bi} of 0.74 V (0.84 V) is obtained for the PEDOT:PSS /Au (Ag). Using $\phi_{anode} = 5.2$ eV one arrives at workfunctions 5.2 – 0.74 eV = 4.46 eV for Au and 5.2 – 0.84 eV = 4.36 eV for Ag. Obviously, the workfunction of Ag at a Ag/PCBM diode is in agreement with the literature value, while in the case of Au there is a difference of 0.64 eV. This difference is not due to a charge accumulation zone next to the electrode but due to the formation of a dipole layer between metal and dielectric as evidenced by photoemission spectroscopy (see Section 2.4.4) (Box 3.4). In the next step, one evaluates the temperature dependence of the injection current. Application of the Arkhipov *et al.* theory [20] to model this field dependence, yields injection barriers of 0.76 eV for Au and 0.65 eV for Ag. Note that if one plotted the data for the temperature of the injection current on a conventional Arrhenius scale applying the Richardson–Schottky model, one would end up with a barrier of only 0.34 eV! The sum of V_{bi} and the injection barrier, that is, 0.74 V + 0.76 eV = 1.50 eV in the case of Au and 0.84 V + 0.65 V = 1.49 eV for Ag, is independent of the metal. This fact is a gratifying confirmation of the injection model because when raising the workfunction of the injecting electrode the injection barrier has to decrease by the same amount by which the open circuit voltage increases.

Box 3.4 Interfacial Dipoles Probed by Photoemission Spectroscopy

The workfunction of an electrode in a diode structure can deviate considerably from the literature value due to specific interfacial effects. In the early days of organic semiconductor physics, it had tacitly been assumed that the barrier for injection of holes from a metal to the semiconductor is indeed the difference between the ionization potential – approximated by the HOMO level – and the literature value for the metal workfunction. This notion is referred to the so-called Schottky–Mott limit in inorganic semiconductor physics [5]. However, when defining the metal workfunction as the minimum energy required for an electron to be emitted into vacuum one observes that this energy depends on the kind of emitting surface. For instance, the workfunction of a tungsten single crystal is 4.63, 5.25, and 4.47 eV for the (100), (110), and (111) surfaces [27]. Since the Fermi level itself must be independent of the crystallographic direction one has to conclude that the escape of an electron from the Fermi level must depend on the crystallographic face. The reason is that the electron wavefunction has a short tail that extends into vacuum and this depends on the kind of surface. It creates a surface dipole because the negatively charged electron cloud above the surface must be compensated by positive countercharges inside the solid. Such a dipole layer will be modified when the surface is covered by organic molecules. Therefore, the energy barrier for injection of either an electron or a hole from a metallic electrode into an organic semiconductor, estimated based on the literature value for the workfunction, needs to be corrected by the surface potential of the dipole layer.

An appropriate technique to assess the magnitude of this dipole layer is photoelectron spectroscopy (UPS or XPS, see Section 2.4.4 [28, 29]). In such an experiment, one measures the kinetic energy spectrum of the emitted electrons at a fixed incident photon energy $h\nu$. The crucial quantity is the maximum kinetic energy, that is, the cut-off energy, of the emitted electrons. For a clean metal surface this is $E_{max} = h\nu - \phi_m$, where ϕ_m is the workfunction of the metal. Suppose that a thin organic layer is deposited on top of a metal. Let the organic layer be thin enough so that

Samsung Exhibit 1058, Page 27 of 33
Samsung v. W&Wsens - PGR2025-00082

the emitted metal electrons penetrate the organic layer without appreciable energy loss. One observes a superposition of the emission that originates from the metal electrons and from electrons from the HOMO level of the organic layer. If the organic layer creates interfacial dipoles, this will give rise to a surface potential ϕ_s. If ϕ_s is negative, the cut-off energy of the metal electrons is diminished by Δ because they originate from deeper states of the Fermi level. Therefore, the difference between the cut-off energies of the metal electrons with and without the organic layer is a direct measure of Δ and, concomitantly, of the workfunction of the metal at the interface. Since electrons emitted from the organic layer do not have to penetrate the interfacial dipole layer their cut-off energy is $h\nu - I_E$ where I_E is the ionization potential of the organic layer. By this token one determines I_E as well as the energy barrier between the Fermi level of the metal and the HOMO of the organic layer. An example is the work by Kahn *et al.* [30]. Those authors found that upon depositing a 0.4–2.0 nm thick layer of α-NPD, that has an ionization energy of 5.4–5.5 eV, on a top of a ultra-pure clean Au electrode the workfunction decreases from 5.2 to 4.0 eV because a dipole layer is formed that causes a potential drop as large as −1.2 eV. This layer raises the hole injection barrier from 0.2 eV that one expected when the Au workfunction was 5.2 eV to 1.3 eV.

It turns out that dipoles are ubiquitous at interfaces between metals and organic materials [31–34]. They are also responsible for the deviations from the literature value for the metal workfunctions inferred from photoemission experiments on metal surfaces that had been exposed to air. There are several origins for those dipoles. There can be (i) partial charge transfer (CT) based upon the position of the ionization potential and electron affinity of the organic layer relative to the workfunction of the electrode, (ii) a chemical reaction that gives rise to the formation of gap states that pin the Fermi level at the interface, and (iii) a modification of the metal electrode due to the presence of the organic layer [30]. In this context, it is worth commenting on the notion of possible band bending close to the interface of the organic dielectric [26]. In inorganic semiconductors, such band bending occurs frequently because of charge flow from the semiconductor to the electrode that establishes the common Fermi level. However, in view of the large electrical band gap in common organic solids, there are no free charges that could be transferred to the electrode and, concomitantly, there can be no band bending except when the electrode forms an ohmic contact able to sustain an SCL current. Band bending also occurs in doped organic semiconductors [35].

The existence of a dipole layer at a metal-organic interface is an unfortunate effect when trying to form an ohmic contact using a high workfunction material such as gold. One can circumvent this problem by replacing the metal by a PEDOT:PSS electrode. Depending on their preparation their workfunction can be comparable to that of a clean gold electrode but the dipole effect is minimal [30].

In addition to Arkhipov's approach in 1999 for describing injection into a disordered semiconductor, other models have been developed. In 2000, Burin and Ratner [36] presented an injection model based on the idea that injection and transport occur through one-dimensional straight paths, effectively lowering the injection barrier. Meanwhile, van der Holst *et al.* [37, 38], developed a three-dimensional Master equation model that includes the disorder in the transport and avoids the shortcomings of the one-dimensional model, in which carrier blockade events can be crucial. It is fair to say, though, that for devices operating close to room temperature, the more simple treatment of Arkhipov *et al.* is sufficient. It is worthwhile to point out, however, that all these treatments rely on the notion that the initial injection event is largely controlled by the existence of tail states of the DOS at the interface and that this is defined by an energy versus hopping range optimization procedure. Since in a bulk system, the low energy sites are spatially fixed, the injection process is NOT spatially homogeneous, but filamentary as pointed out by van der Holst *et al.*

Samsung Exhibit 1058, Page 28 of 33
Samsung v. W&Wsens - PGR2025-00082

4
Fundamentals of Organic Semiconductor Devices

By definition, semiconductor materials are intended to be used in semiconductor devices. We shall therefore consider here the operational principles of some elementary devices, that is, organic solar cells (OSCs), organic light-emitting diodes (OLEDs), and organic field-effect transistors (OFETs). Our purpose is to give a basic introduction for those not yet familiar with the operation of organic semiconductor devices. Eventually, the reader should be in a position to enjoy the numerous dedicated book chapters and review articles available that treat these devices at an advanced level with regard to the current state of the art and its further improvement.

From the discussion of the previous chapters on the nature of and processes with excited states and charges in organic semiconductors, it should be evident that one would be ill-advised to simply take equations from an inorganic semiconductor textbook and use them for the operation of organic devices. The inorganic semiconductor equations have been derived for certain conditions that are not always met in organic materials. Some of the underlying presumptions for the inorganic semiconductor equations are:

a) In inorganic semiconductors, there is a high intrinsic density of charge carriers at room temperatures. In contrast, organic "semiconductors" are essentially insulators, having no intrinsic mobile charge carrier density (see Section 2.4.1). For example, using $n_i(T) = N_{eff}e^{-E_g/2kT}$, the intrinsic carrier density at room temperature in silicon, germanium and gallium arsenide can be estimated as $9\times10^9\,cm^{-3}$, $2\times10^{13}\,cm^{-3}$, and $2\times10^6\,cm^{-3}$, respectively. In contrast, in organic materials, the intrinsic carrier density is $\approx 0\,cm^{-3}$. To convince oneself, take the typical molecular density of $10^{21}\,cm^{-3}$ for N_{eff} and a typical gap of 3 eV. The situation changes upon doping or charge injection under space charge limited conditions. Then, charge carrier densities can become comparable to those in inorganics. In doped inorganic materials, the carrier density tends to be around $10^{15}-10^{18}\,cm^{-3}$, depending on the doping level [1, 2]. Such charge densities can also be obtained in organic semiconductors, for example when a potential of 1 V is applied across a 100 nm thick film, so that charges are injected and accumulate in the case of space charge limited current of one carrier type. As detailed in Section 3.1.2, eq. 3.10, the associated charge carrier density is $n = (3/2)(\varepsilon_0\varepsilon_r/e)(F/d) = 3\times10^{16}\,cm^{-3}$. Space charge limited current prevails in OLEDs, yet not in OSCs. Similarly, the density of holes upon doping zinc-phthalocyanine with F4-TCNQ has been estimated to range from 10^{15} to $10^{19}\,cm^3$, depending on the doping level [3]. Note though that obtaining stable p and n-type doping in organic semiconductors is, however, still a challenge that is under current development.
b) In inorganic semiconductors, the charge carriers have a high mobility. Typical mobilities in inorganic semiconductors are in the range of $10^3-10^4\,cm^2\,V^{-1}\,s^{-1}$. In contrast, in organic semiconductors, mobilities range from about $10^{-5}-10^{-2}\,cm^2\,V^{-1}\,s^{-1}$ for amorphous materials [4], with the higher value of up to $10\,cm^2\,V^{-1}\,s^{-1}$ for crystalline materials such as rubrene in OFETs [5].
c) In inorganic semiconductors, the current flow results mainly from diffusion current, with drift current playing a minor role. *Diffusion current* results from a spatial gradient of charge density

Electronic Processes in Organic Semiconductors, First Edition. Anna Köhler and Heinz Bässler.
© 2015 Wiley-VCH Verlag GmbH & Co. KGaA. Published 2015 by Wiley-VCH Verlag GmbH & Co. KGaA.

Samsung Exhibit 1058, Page 29 of 33
Samsung v. W&Wsens - PGR2025-00082

while *drift current* originates from a spatial gradient in the electric field. In inorganic semiconductors, the diffusion current controls, for example, the formation of a pn-junction or a Schottky junction (see Boxes 4.1 and 4.2). In contrast, in organic semiconductors, diffusion current is insignificant (with the exception of OSC at voltages close to the open-circuit voltage, see below), and the operation of OLEDs, OSCs and OFETs relies mainly on drift current.

d) In inorganic semiconductors, absorption of light creates free charge carriers. As a consequence, the photocurrent adds as a voltage-independent term to the Shockley equation that describes the current–voltage curve of an inorganic solar cell (Box 4.1). In contrast, in organic semiconductors, the creation of mobile charge carriers from the dissociation of photoexcited excitons has a strong dependence on the electrical field, as detailed in Chapter 3. This is a major, if not even the main factor controlling the current–voltage characteristics of an OSC.

These few examples may suffice to illustrate that care and good judgement are needed when quantitatively describing the operation of organic semiconductor devices.

Box 4.1 The pn Junction and the Shockley Equation

Inorganic semiconductor solar cells, such as the ones made from crystalline silicon or germanium, are based on a device architecture that uses a pn-junction or a Schottky junction. In both cases, a depletion zone is formed. By considering the thermally activated diffusive flow of minority charge carriers across the depletion zone, Shockley [6] was able to derive an equation describing the current,

$$j(V) = j_0 \left(\exp\left(\frac{qV}{\eta kT} \right) - 1 \right) \tag{B4.1.1}$$

η is an ideality factor, taking the value of 1 for ideal cells and values exceeding 1 if recombination processes prevail. q is the electric charge, V is the applied voltage, k and T take their usual meaning as Boltzmann constant and temperature. j_0 is the recombination current that remains at high reverse bias. When such diodes are illuminated, the photocurrent j_{ph} adds as a constant, voltage-independent term.

$$j(V) = j_0 \left(\exp\left(\frac{qV}{\eta kT} \right) - 1 \right) + j_{ph} \tag{B4.1.2}$$

This is well justified since, for crystalline inorganic semiconductors, the creation of free, mobile charges by light absorption is independent of the applied current. In a real solar cell, there are losses that may be modeled as a series resistance R_s and a parallel (shunt) resistance R_p. Factors that give rise to a series resistance include the contact resistance of the electrodes or the sheet resistance of semiconductor bulk. A parallel resistance may arise from alternative current pathways around the diode. These resistances can be included to give

$$j(V) = j_0 \left(\exp\left(\frac{q\left(V - jR_s\right)}{\eta kT} \right) - 1 \right) + j_{ph} + \frac{(V - jR_s)}{R_p} \tag{B4.1.3}$$

Figure B4.1.1 shows the characteristic of an ideal diode and of diodes with a series or shunt resistance. The associated circuit diagram is shown as well.

In order to appreciate when the Shockley equation may appropriately be used to describe the current–voltage characteristics, it is instructive to recall its derivation, for example, in the context of a pn junction. The physics of the pn-junction and of the Schottky junction can be found in full mathematical detail in any semiconductor physics textbook, and also in most solid state physics textbooks, for example, [7]. For the sake of readers without an extensive background in physics, we briefly summarize the salient points. An inorganic p-type semiconductor consists of

Samsung Exhibit 1058, Page 30 of 33
Samsung v. W&Wsens - PGR2025-00082

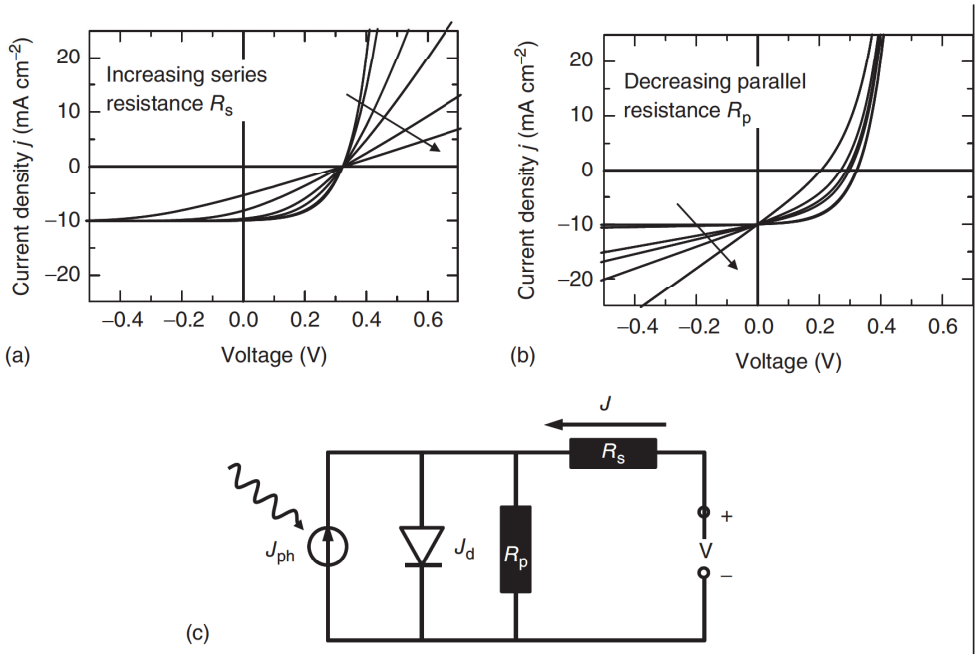


Figure B4.1.1 (a) The effect of increasing the series resistance R_s on the current–voltage curves according to Eq. (B4.1.3) (for $\eta = 1$, $R_p = \infty$). (b) The effect of decreasing the parallel (shunt) resistance R_p on the current–voltage curves according to Eq. (B4.1.3) (for $\eta = 1$, $R_s = 0$). (c) The equivalent circuit diagram fora real solar cell with a series resistance R_s and a parallel (shunt) resistance R_p.

a crystal containing dopants that can accept electrons, thus releasing holes. Similarly, a n-type semiconductor is doped with elements that release electrons. At room temperature, most of the dopants are ionized. Overall, the p-type and the n-type semiconductor are both charge-neutral. When they are brought in contact, electrons will diffuse from the n-type semiconductor into the p-type one and vice versa. This diffusion is driven by the gradient of charge concentration. Since electrons leave the previously neutral n-type semiconductor, it becomes positively charged. The same applies inversely to the p-type region. As a result, an electric field builds up that prevents further diffusive loss of electrons (Figure B4.1.2). Shockley now considered the detailed balance of carrier flow in equilibrium [6]. He argued that a hole may happen to diffuse from the p-type region into the n-type region until they are captured by a recombination center. In doing so, it diffuses into an area of higher potential energy (Figure B4.1.2). The probability of this diffusion happening depends exponentially on the ratio between the build-in potential barrier that the hole aims to surmount and its thermal energy kT. This leads to a current $j^{o,p}$. When a positive voltage V is applied, the barrier is diminished by an amount qV and the current increases correspondingly. In addition recombination centers in the n-type region may release holes that then move energetically downhill into the p-type area with a probability of 1. The total flow of hole current from the p to the n type area is then given by

$$j(V) = j_{0,p}\left(\exp(\left(\frac{qV}{\eta kT}\right) - 1\right) \qquad \text{(B4.1.4)}$$

where $j_{0,p}$ is the saturation current of holes that prevails at a high negative bias. The same argument can be brought forward for the current resulting from electrons moving from the n-type area into the p-type region. The two currents add up to give Eq. (B4.1.1), with the total saturation current being composed of both the hole and electron current. The key point to take away

from this derivation is that it is derived by considering the detailed balance of a diffusive current flow. This applies to semiconductors having a sufficient number of mobile charge carriers that can diffuse.

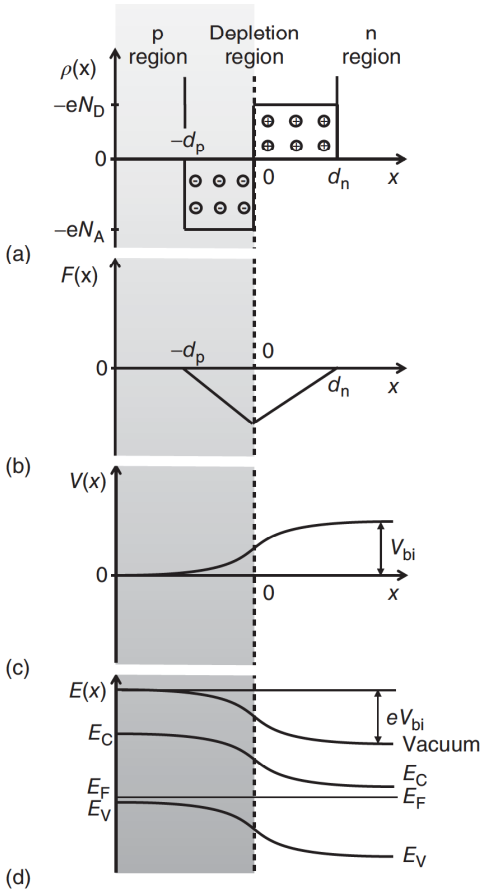


Figure B4.1.2 The Schottky-model for a pn-junction in the limit that the doping concentration between the p-type and n-type region changes abruptly (*abrupt junction approximation*). The area of the p-type material is shaded gray and that of the n-type material is allowed to remain in white. (a) Spatial variation of the space-charge density $\rho(x)$ produced by ionized acceptors N_A and donors N_D. A depletion ranging from $-d_p$ to d_n has formed as a result of diffusion. (b) The resulting distribution of the electric field strength $F(x)$. (c) The associated spatial variation of the electric potential (x). (d) The resulting spatial variation of the energy band diagram. Note how the Fermi energies align. Outside the depletion region, the energy difference between valence band edge and Fermi level, or conduction band edge and Fermi level, remains unaltered while this varies within the depletion region.

4.1
Basic Solar Cells and Light-Emitting Diode Structures

In order to make a device, an organic semiconductor material needs to be connected to two different electrodes. There are two fundamentally distinct geometries how this can be obtained (Figure 4.1).

a) In a lateral arrangement (Figure 4.1a), both electrodes are on the same side of the organic semiconductor, so that the current flows parallel to the semiconductor surface. To maximize the active size of the device, the electrodes are positioned in an interdigitated way. Today, this interdigitated-type device structure arrangement is rarely used for OSCs and OLEDs, mainly because the charge flow is limited to a few layers of material near the surface. The resulting high charge density enhances unwanted bimolecular processes. In addition, the surface is prone to contamination by oxygen or water. In contrast, for OFETs, the lateral arrangement is the standard geometry. A third "gate" electrode on the other side of the organic semiconductor, separated from it by an insulating layer, is used to control the amount of current flowing between the two lateral electrodes (Figure 4.1b). Light-emitting OFETs can also be fabricated using this geometry when the transistor is made to be ambipolar for a light-emitting material. In that case, the simultaneous flow of electrons and holes results in an emission zone in between the two lateral electrodes [8, 9].
b) In the more common vertical "sandwich-type" arrangement, the organic semiconductor is sandwiched between the two electrodes, and current flows perpendicular to the semiconductor surface, through the bulk of the semiconductor film (Figure 4.1c). The sandwich-type device structure is the one considered in the subsequent sections.

4.1.1
Basic Fabrication Steps

The semiconductor and the electrodes need to be supported by a substrate. For eventual consumer-oriented applications, a transparent flexible plastic foil may be used. For every-day laboratory work, it is more convenient to use a glass substrate. For practical reasons, the most common choice for the bottom electrode, usually being the anode of the device, is to use a transparent conductive oxide such as indium-tin-oxide (ITO), though other transparent conductive oxides like SnO_2, ZnO, ZnO:Al (ZnO doped with Al), MoO_3, or others may be used as well. ITO is an indium oxide, In_2O_3, doped with up to 9 mol% of tin, therefore also written as In_2O_3:Sn. Fan and Goodenough [10] describe it as a heavily doped, degenerate crystalline semiconductor. They suggest that the conduction band

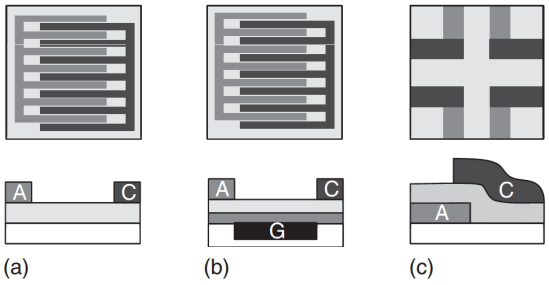


Figure 4.1 Device geometries of organic semiconductor devices (top view and side view). (a) Structure with interdigitated electrode (anode A and cathode C) on top of an organic semiconductor film covering a glass substrate. This structure is rarely used. (b) Structure with interdigitated top electrodes and a bottom gate (G). This structure is common for OFETs. (c) Four structures on a glass substrate where the organic semiconductor film is sandwiched between the anode (A) and the cathode (C). The side view shows only one of the four structures.

Samsung Exhibit 1058, Page 33 of 33
Samsung v. W&Wsens - PGR2025-00082